Deep Neural Network for Detecting Nucleon-Nucleon Bound States

Denny Lane B. Sombillo
National Institute of Physics
University of the Philippines Diliman
Quezon City, 1101 Philippines
dbsombillo@up.edu.ph

Research Center for Nuclear Physics
Osaka University
Osaka 567-0047, Japan
sombillo@rcnp.osaka-u.ac.jp

Abstract

There is a long-standing ambiguity in the interpretation of near-threshold enhancement in hadron-hadron scatterings. The origin of enhancement can reveal the nature of the interaction between the two hadrons. However, there is no straightforward approach to probe the nature of near-threshold enhancement in a model-independent manner. The present study aimed to formulate a deep learning approach to detect a two-hadron bound state given only the partial scattering cross-section. To ensure that analyticity and unitarity were satisfied, an S-matrix model with a parameterized background was used for the training dataset. A deep neural network (DNN) model was designed and developed using the Adam and AMSGrad optimizers. To demonstrate that the trained DNN model can generalize beyond the training dataset, two variants of exact amplitudes of separable potential were used for validation. Finally, without using the deuteron's known properties, such as the binding energy and its magnetic moment, the model identified the correct origin of threshold enhancement in the nucleon-nucleon scattering data. The proposed method can be applied to analyze the recently discovered near-threshold enhancements observed in scattering experiments.

1. Introduction

One of the possible candidate quantum states of near-threshold enhancement observed in hadron-hadron scatterings are hadronic molecules or enhanced kinematical effects (Guo *et al.*, 2018; Guo *et al.*, 2015; Olsen *et al.*, 2018;

Yamaguchi *et al*., 2020). These molecular states are generated by the dynamics of meson exchange with heavier mesons responsible for the intricate balance between short-range attraction and repulsion. On the other hand, the generally attractive long-distance behavior is dominated by the exchange of lighter meson (i.e., the pion). All the stable and unstable nuclei fall under the molecular hadron category. However, unlike in nuclear physics, the more general hadronic molecules are expected to be unstable. This short-lived nature of unstable hadronic molecules prevents a direct study of their properties and the only possible direction to make progress is to use the scattering data.

In this paper, a deep neural network (DNN) was constructed that can detect the nucleon-nucleon-bound state using only the scattering cross-section. The proposed approach is crucial in interpreting near-threshold phenomena because, as stated, resonances are short-lived and cannot be studied directly. The low energy scattering of two nucleons provides a benchmark where the deep learning approach can be tested. Two S-wave cross-sections associated with nucleon-nucleon scattering were used: the spin-singlet and the spin-triplet shown in Figure 1.
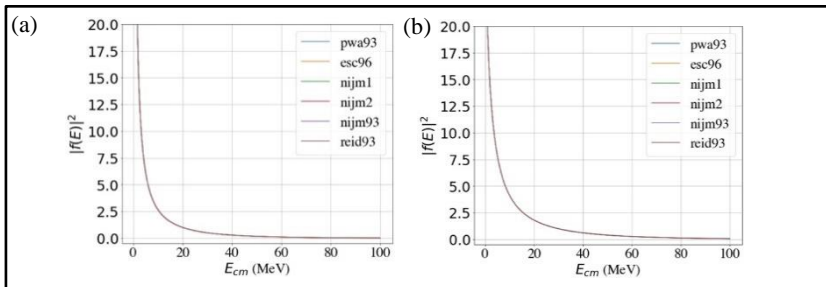

Figure 1. S-wave partial cross-sections of nucleon-nucleon in spin singlet (a) and spin triplet (b) configurations

PWA93 corresponds to the analyses of the multi-energy partial wave of the nucleon-nucleon system (Stoks *et al*., 1993). ECS96 is a two-meson-exchange model that reproduces the nucleon-nucleon scattering data (Rijken *et al*., 1996). Nijm93 is the Nijmegen soft-core potential for which the NijmI is the nonlocal version, while NijmII is the local version (Stoks *et al*., 1994). Finally, Reid93 corresponds to the regularized soft-core potential (Stoks *et al*., 1994). All these analyses and models reproduced the nucleon-nucleon scattering data very well with $\chi^2 / ndf \sim 1$. In the energy window considered in the present study, all the data to be analyzed were almost overlapping as seen in Figure 1, which reflects the consistency of the different approaches. The data in Figure 1 are obtained from Stoks *et al*. (1993, 1994) and Rijken *et al*. (1996).

Note that the spin-singlet and the spin-triplet cross-sections exhibited large values at the threshold ($E_{cm} = 0$), suggesting a possible nucleon-nucleon molecular state. The precise knowledge of deuteron's binding energy and magnetic moment can be used to deduce that the spin-triplet threshold enhancement corresponds to the two-nucleon-bound state. Specifically, it is known that the deuteron's binding energy is around 2.2 MeV and the S-wave spin-triplet component dominates the deuteron's wave function. Unlike in the deuteron, where the neutron and proton form a stable composite hadron, hadronic resonances are short-lived and the only way of inferring their existence and properties is through the scattering experiment. To simulate the ignorance of near-threshold resonances, a method is proposed to identify which of the threshold enhancements in Figure 1 is caused by a bound state without using the known properties of the deuteron.

The objective of the study can be explicitly stated as follows: given a collection of S-wave scattering cross-sections, how to detect if the observed threshold enhancement is caused by a physical state? This makes deep learning a viable tool in the study of near-threshold phenomena. Machine learning techniques are an indispensable tool used in physical sciences (Carleo *et al*., 2019). Surprisingly, it is not yet applied to analyze near-threshold phenomena except in the work of Sombillo *et al*. (2020) where the general single-channel scattering was studied. In this work, a large size of training dataset was generated to solve the classification problem. The scattering data were then used to infer the existence of a nucleon-nucleon-bound state.
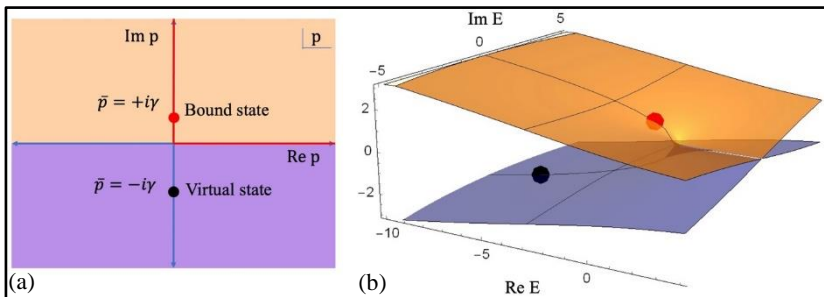
2. Methodology

2.1 Simulating the Analytic Structure of S-matrix

The S-matrix contains all the information that one needs about the interactions between two scattering hadrons. However, due to quantum chromodynamics' nonperturbative nature in the low energy regime, the exact form of the S-matrix cannot be derived. Nevertheless, there are general properties that must be satisfied by the S-matrix. First, causality (i.e., the scattering cannot precede the collision) implies that the scattering amplitude should be analytic in the first quadrant of the complex momentum plane (van Kampen, 1953; Eden *et al*., 1966). Imposing analyticity on the S-matrix means that there should be no singularities on the upper half of the complex momentum plane, except along the imaginary axis. Next is that the probability conservation requires that the

S-matrix be unitary. Guided by the analyticity, one can start with the condition that determines the amplitude's singularities and then use unitarity to deduce the complete form of the S-matrix. By using all the parameters in the present study's constructed model, a sizable training dataset can be generated.

Actual scattering phenomena happen on the real momentum line. However, by allowing the scattering amplitude to take complex-valued momentum or energy, one can access useful information about the spectral properties of the physical process. The bound state corresponds to the simple pole on the positive imaginary momentum axis of an analytically continued scattering amplitude as shown in Figure 2a. The corresponding poles on the complex energy plane are shown in Figure 2b. The asymptotic solution $\psi_{\bar{p}}(r)$ to the Schrödinger equation (Equation 1) has an exponentially decaying tail if $\bar{p} = i\gamma$ where $\gamma > 0$.

$$\psi_{\bar{p}}(r) \to \frac{1}{r} e^{i\bar{p}r} = \frac{1}{r} e^{-\gamma r}; \quad r \to \infty \tag{1}$$

The red dots correspond to the bound state pole while the black dots to the virtual state pole.

Figure 2. Bound and virtual state poles on complex momentum plane (a) and complex energy plane (b)

A large scattering cross-section at the threshold is one manifestation that the colliding particles can form a bound state. However, a pole in the negative imaginary axis can also produce a large cross-section at the threshold. Reversing the sign of γ in Equation 1 gives a nonnormalizable wave function. This state is called a virtual state because it cannot represent a physical state and its only significance is that it gives a large enhancement at the threshold in the scattering cross-section (Taylor, 1972).

Looking at the partial cross-sections in Figure 1, it would be very hard, if not impossible, to distinguish the two enhancements with two completely different physics without using the known properties of the deuteron. To help

the DNN distinguish the two structures, an S-matrix parametrization in momentum representation was introduced in Equation 2.

$$S(p) = exp\left[2i\eta\, tan^{-1}\left(\tfrac{p}{\Lambda}\right)\right]\left(\frac{p+i\gamma_{far}}{p-i\gamma_{far}}\right)\left(\frac{p+i\gamma_{near}}{p-i\gamma_{near}}\right) \qquad (2)$$

where the first factor, containing the η and the Λ parameters, is the background singularity simulating the left hand-cut in the scattering energy plane. The η determines whether the background is attractive or repulsive, while Λ controls how far the background is from the threshold. The second factor simulates a simple pole background through the parameter γ_{far}. The third factor is responsible for the threshold enhancement in the simulated cross-sections. If $\gamma_{near} > 0$ one gets a bound state pole enhancement. Otherwise, the enhancement is due to a virtual state pole. The relevant partial scattering cross-section was obtained using the relation in Equation 3.

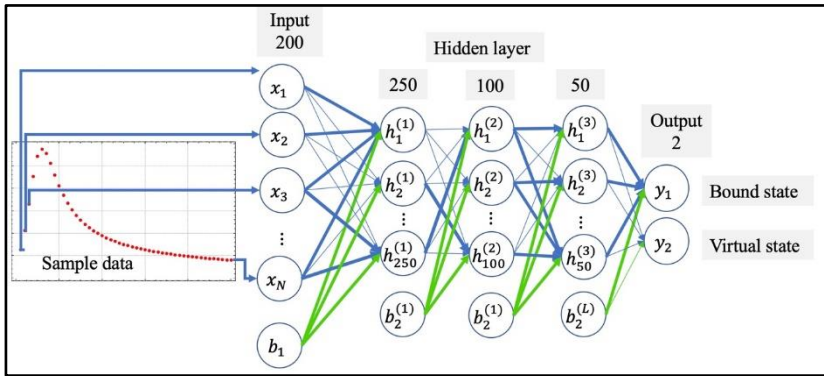$$|f(p)|^2 = \left|\frac{S(p)-1}{2ip}\right|^2 \qquad (3)$$

In the construction of cross-sections, the non-relativistic relation $E = p^2/2\mu$ was used where μ is the reduced mass of two hadrons. Since one can control the sign of γ_{near}, each cross-section can be appropriately labeled.

A large size of the training dataset was generated by choosing random values of all the parameters in Equation 2. Specifically, 10 random values of η in the interval $(-4, -1)$ to simulate a repulsive background were generated. The repulsive background was chosen to mimic the Pauli spin blocking effect. After which, 20 random values of Λ were generated within the range $(500, 700$ MeV$)$. The distance of the background from the threshold was deliberately limited for the later numerical experiment. Now, 1,000 random values of γ_{near} were generated within the interval $(-0.9\,\Lambda, 200$ MeV$)$. It was ensured that the γ_{near} is the closest singularity to the threshold by limiting its lower bound based on the value of Λ. Also, nucleon-nucleon potential is not very deep to create a bound state with very high binding energy. Thus, a maximum of 200 MeV will suffice. Finally, 20 values of γ_{far} were generated in the interval $\left(-2.0\Lambda, -|\gamma_{near}|\right)$. This interval was chosen to ensure that γ_{near} is the nearest pole singularity. Overall, 4×10^6 labeled cross-sections were produced. Only 3.2×10^6 of these labeled cross sections were used for the direct training and kept the remaining 8×10^5 for the testing.

One can readily recognize the importance of background singularities. If only $S(p) = (p + i\gamma_{near}) / (p - i\gamma_{near})$ is used, the cross-section becomes $|f(p)|^2 = 1/(p^2 + \gamma_{near}^2)$. That is, there is no way to distinguish the cross-sections using only the sign of γ_{near}. Without the background, the bound and virtual cross-sections are identical. The effect of background on the distinguishability of bound and virtual enhancements can directly affect the present DNN models' performance.

2.2 Optimization of DNN Model

The DNN architecture is shown in Figure 3 with the input layer containing 200 nodes, three hidden layers with 250, 100 and 50 nodes, and 2 output nodes. The input layer will take the cross-section values on the energy points (0, 100 MeV). Other architectures were considered in a previous study (Sombillo, *et al.*, 2020) and found that the hidden layer with architecture (250-100-50) performed better than the other architecture considered in the same study. The full analysis and the codes used are accessible in the author's online code repository (Sombillo, 2020).

The blue connection lines represent the weights while the green lines are the biases.

Figure 3. The DNN architecture used in this study

The hidden layer-nodes are equipped with rectified linear unit (ReLU) activation function and the output nodes with softmax. The chosen activation functions are appropriate for the classification problem because ReLU can minimize the vanishing of gradient and is much faster to compute compared with the functional call like in sigmoid activation. Softmax, on the other hand, has an automated way to minimize the activation of the wrong nodes and enhance the correct node, which is important in the classification problem.

The softmax cross-entropy was used as the cost function to match the softmax node in the output layer.

The objective of the training was to get the optimal values of weights and biases that minimize the cost function. The training usually proceeded by feeding all the training datasets to the network to approximate the present state of the cost function. This is referred to as the forward pass. Then, the values of weights and biases were updated using some variant of gradient descent. In this study, two commonly used optimizers: Adam (adaptive moment) and AMSGrad (a variant of Adam) were used. The Adam is a first-order gradient optimization based on adaptive estimates of lower-order moments (Kingma and Ba, 2015). The AMSGrad, on the other hand, is a variant of Adam that enforces the learning rate matrix to be decreasing (Reddi *et al*., 2018). Both Adam and AMSGrad offer fast convergence which was essential for the present task. The construction of the DNN model, the hyperparameter settings of optimizers, and the training loop were made using Chainer (Tokui *et al*., 2015; Akiba *et al*., 2017; Tokui *et al*., 2019).

The performance of the DNN was improved by executing several training epochs. Here, one epoch corresponded to one complete forward pass and backpropagation of the entire training dataset. The mini-batch system was used in the forward pass to introduce stochasticity in the cost-function calculation. Figure 4 shows the performance of the present work's DNN model using two optimizers during the training process. The blue lines represent the model's performance on the training dataset, while the orange lines are for the testing set.
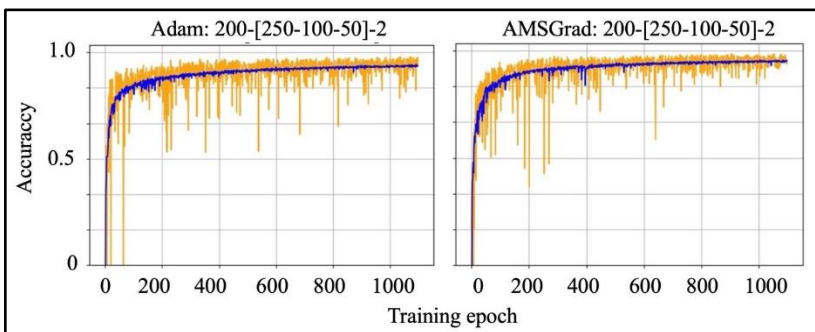

Figure 4. The training and testing performance of the DNN

Notice that both the training and testing monotonically increased as the training progresses. There was no essential difference between the performance using two different optimizers. This implied that the optimization was not overfitting the parameters and the DNN achieved generalization within the training dataset. After 1,100 training epochs, 99.805 and 99.928% for the testing and training accuracies were obtained in Adam optimization, respectively. For the AMSGrad, 99.859 and 99.823% for the training and testing, respectively were achieved. Tables 1 and 2 show the confusion matrix for the corresponding trained model on the training and testing datasets. The result showed that the difficulty of identifying a bound state enhancement was comparable with that of the virtual enhancement.

Table 1. Confusion matrix for the trained DNN Adam:200-[250-100-50]-2

Total number of training items: 3,200,000		
True bound states: 1,600,000	Inferred bound states: 1,596,753	Inferred not bound states: 3,247
True virtual states: 1,600,000	Inferred virtual states: 1,596,847	Inferred not virtual states: 3,153
Total number of testing items: 800,000		
True bound states: 400,000	Inferred bound states: 399,725	Inferred not bound states: 275
True virtual states: 400,000	Inferred virtual states: 399,715	Inferred not virtual states: 285

Table 2. Confusion matrix for the trained DNN AMSGrad:200-[250-100-50]-2

Total number of training items: 3,200,000		
True bound states: 1,600,000	Inferred bound states: 1,596,768	Inferred not bound states: 3,232
True virtual states: 1,600,000	Inferred virtual states: 1,596,752	Inferred not virtual states: 3,248
Total number of testing items: 800,000		
True bound states: 400,000	Inferred bound states: 399,286	Inferred not bound states: 714
True virtual states: 400,000	Inferred virtual states: 399,274	Inferred not virtual states: 726

The training of the DNN model above was based on the following numerical experiments. First, the inference capabilities of the DNN models were validated using the separable potential. It was important to ensure that the cross-sections of the validation set were independent of the training dataset. Then, the validated DNN models were deployed to analyze the nucleon-nucleon scattering data.

2.3 Validation of the Trained DNN

One of the promises of the deep learning approach is that a trained DNN model can generalize beyond the training set. It is, therefore, fitting to verify generalization before deploying the models to extract information from the experimental data. The author generated a set of independent cross-sections using the separable potential model. This kind of potential is expected for the nucleon-nucleon system because the interaction is short-ranged and highly dependent on momentum.

2.3.1 Cross-Sections for the Separable Potential

In the S-wave, a non-local potential in momentum representation took the form of Equation 4.

$$v(p, p') = \zeta \left(\frac{\Lambda^2}{p^2 + \Lambda^2} \right) \left(\frac{\Lambda^2}{p'^2 + \Lambda^2} \right) \tag{4}$$

where Λ is the cut-off parameter associated with the Yamaguchi form-factor while ζ is the coupling strength (Yamaguchi, 1954; Pearce and Gibson, 1989). The same symbol for the cut-off parameter in Equations 4 and 2 is used because both are related to the background singularities.

The scattering amplitude was obtained by solving the Lippmann-Schwinger equation (Equation 5).

$$f(p, p') = v(p,p') + \int_0^\infty dp'' \, p''^2 v(p,p'') \frac{1}{E - p''^2/2\mu + i\epsilon} f(p'',p'') \tag{5}$$

where p and p' are the incoming and the outgoing relative momenta, and p'' is the off-shell momentum. Using the relation in Equation 3, the corresponding S-matrix takes the form in Equation 6.

$$S_{ind}(p) = \left(\frac{p + i\Lambda}{p - i\Lambda} \right)^2 \left[\frac{2(p - i\Lambda)^2 - \zeta\pi\mu\Lambda^3}{2(p + i\Lambda)^2 - \zeta\pi\mu\Lambda^3} \right] \tag{6}$$

Inspection of the denominator in Equation 6 tells that for negative ζ (attractive potential), exactly one bound state pole can be produced. This is a general feature expected from a separable potential (Newton, 1982). The S-matrix in Equation 6 is called the energy-independent coupling model since ζ is just a constant.

In the work of Sombillo (2020), another separable potential was utilized to build a validation set of cross-sections. From Equation 6, it is not possible to produce resonance with attractive potential because of the absence of a centrifugal barrier in the S-wave (Pearce and Gibson, 1989). Thus, the coupling parameter was assigned to have some energy dependence to produce resonance. The energy dependence should be on-shell so that the coupling does not have to participate in the evaluation of the loop integral in Equation 5. The resulting S-matrix when ζ is replaced with $(E - M_{sep})\,\zeta$ is given in Equation 7.

$$S_{dep}\,(p) = \left(\frac{p + i\Lambda}{p - i\Lambda}\right)^2 \left[\frac{2(p - i\Lambda)^2 - (E - M_{sep})\,\zeta\mu\Lambda^3}{2(p + i\Lambda)^2 - (E - M_{sep})\,\zeta\mu\Lambda^3}\right] \qquad (7)$$

where E is the on-shell center-of-mass scattering energy and M_{sep} is some parameter to define the zero of amplitude. In this paper, Equation 7 is referred to as the energy-dependent coupling model.

One interesting feature of Equation 7 is that it can produce a bound state pole or a near-threshold virtual state pole with an accompanying background simple pole. Because of this feature, the threshold enhancement produced in Equation 7 is relatively easy to distinguish than those produced by Equation 6.

It must be emphasized here that the S-matrix used to generate the validation cross-sections in Equations 6 and 7 have a second-order background pole while the training dataset S-matrix in Equation 2 has a branch cut background singularity. This means that the validation set is already outside the training dataset and that there is no reason to believe that the trained DNN can still work with Equations 6 and 7.

2.3.2 Numerical Experiment and Discussion

To validate the performance of the trained DNNs, the following numerical experimentation was performed. Using Equation 6, 100,000 cross-sections were produced by randomly selecting values of cut-off parameters within the range [$N*100 \ MeV$, $(N + 1)*100 \ MeV$], where N is some positive integer that was increased in the experiment. It was ensured that equal numbers of bound states and virtual states enhanced cross-sections were produced in the validation dataset. The cross-sections were fed directly to the trained DNNs and the number of correct inferences was counted. The same procedure was used with the S-matrix model in Equation 7.

The result of the numerical experiment is shown in Figure 5. Each horizontal line contains 100,000 cross-sections with the blue lines for the energy-independent model and the red lines are for the energy-dependent model. For low values of Λ ($\Lambda < 300$ MeV), the difference between the background singularities of the validation S-matrix and the training S-matrix manifest as low inference accuracy. This observation suggests that the inferencing power of DNN becomes highly dependent on the actual nature of backgrounds if they are very close to the threshold. Now, letting the Λ of separable potential to be around ($300 < \Lambda < 700$ MeV), high inference accuracy was obtained. Recall that this range of Λ coincided with the range of the same parameter in the training dataset parametrization. At this point, the difference between the two background singularities no longer matters.
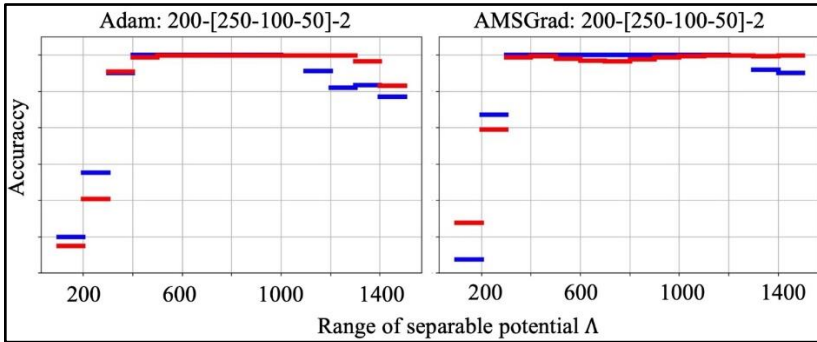

Figure 5. Performance of the trained DNN against the cross-sections generated by separable potential

One surprising result is that even beyond the training range used for Λ, the inference accuracy was still very high. This demonstrates that the trained DNN can generalize beyond the training dataset. Now, at $\Lambda \geq 1000$ MeV, the DNN trained using the typical Adam optimizer started to show some drop in the inference accuracy. Recall that for large Λ, the background singularity was already very far from the threshold and the enhancements produced by a bound state became identical with that of a virtual state. The drop of inference accuracy became more noticeable for the blue lines where the cross-sections were produced by energy-independent coupling. The near-threshold poles of these cross-sections did not have an accompanying simple pole. Thus, the DNN can only rely on the background second-order pole. The decrease in the inference accuracy was mitigated in the case of the red lines where the cross-sections were produced by energy-dependent coupling. Here, the near-threshold pole was always accompanied by a simple pole serving as a nearby background.

3. Results and Discussion

The nucleon-nucleon scattering data used were obtained from the different partial-wave analyses and potential models that fit the data very well (Stoks *et al.*, 1993, 1994; Rijken *et al.*, 1996). The cross-sections on the center-of-mass energies (0, 100 MeV) were generated from the phase shift values in the online interactive repository (Nijmegen Group, 2005). Then, all the cross-sections were fed to the trained DNN to extract the inference output.

The results for both models considered in this study are shown in Table 3. The two DNN models that were considered gave the same inference output for the nucleon-nucleon partial cross-sections and all the results were correct. That is, the spin-singlet cross-section enhancement was correctly identified as due to a virtual state pole and the spin-triplet to a bound state pole. This is surprising because the actual nucleon-nucleon interaction was far more sophisticated than the simple separable potential. Nevertheless, the results showed that the general properties of the S-matrix, using a simple parametrization in Equation 2, are already sufficient to simulate the analytic structure of the nucleon-nucleon S-matrix.

Table 3. Inference output of the two trained DNN

Spin configuration	PWA93 input	ECS96 input	NijmI input	NijmII input	Nijm93 input	Reid93 input
Spin-singlet	Virtual	Virtual	Virtual	Virtual	Virtual	Virtual
Spin-triplet	Bound	Bound	Bound	Bound	Bound	Bound

How does a DNN differentiate the two seemingly similar structures at the threshold of nucleon-nucleon cross-section without using the known properties of deuteron? This is all because of the asymmetry in the possible number of singularities in the upper and lower half of the complex momentum plane. The S-matrix is considered as a meromorphic function of momentum (i.e., it is analytic except at those regions with poles). In addition, analyticity prevents the pole to appear on the upper half of the momentum plane except on the imaginary axis. Thus, all the other poles and singularities are packed together on the lower half-plane. This asymmetry in the distribution of singularities is exploited in the formulation and utilized by the DNN to distinguish the two structures.

This study demonstrated that the general properties of the S-matrix are sufficient to generate the training dataset of a classification DNN. The trained

neural network gives accurate inferences even if the actual data is more complicated than the training dataset. The architectures and the type of optimizers used in the design of the network showed no significant difference. Both trained neural network models can be used to detect bound state given only the scattering cross-sections.

The ability of the present study's trained DNN to detect bound states, given only a cross-section with threshold enhancement, would help in identifying which enhanced signals in the experimental data corresponds to a dynamically generated physical state. However, in addition to dynamically generated states, another possible interpretation of the near-threshold phenomenon is the accidental appearance of a compact resonance state in the vicinity of the threshold. In the recent work of Sombillo *et al*. (2021), DNN that can probe the unphysical Riemann sheet of a coupled-channel scattering and count the number of poles were formulated. The distribution of poles on the different unphysical Riemann sheets can be used to deduce the nature of near-threshold phenomena in accordance with the pole-counting argument of Morgan (Morgan, 1992; Morgan and Pennington, 1993). In particular, if the enhancement is caused by an isolated pole in the second Riemann sheet, then it is most likely dynamically generated. If the pole in the second sheet is accompanied by another pole in the third sheet, then it is most likely a compact quark state resonance. Once the signal is identified to be caused by a physical state, the next step should be the determination of the pole parameters. At this point, a regression-type DNN designed to extract the pole parameters might be worth exploring in future studies.

4. Conclusion

In conclusion, the trained DNN can be used to detect the presence of hadron-hadron bound state given only the scattering data. The difficulty of detection can only happen if the background singularities are far from the relevant threshold. In practical application, the S-matrix always has some background singularities and these can be exploited by the DNN to unambiguously interpret the signal as corresponding to bound state. The obtained accuracy was sufficiently high to unambiguously interpret the nature of threshold enhancement.

5. Acknowledgement

The author would like to thank Prof. Atsushi Hosaka, Prof. Toru Sato and Prof. Yoichi Ikeda for the many insightful discussions. The author's postdoctoral research fellowship is supported in part by the University of the Philippines Office of the Vice President for Academic Affairs (OVPAA) Faculty, REPS and Administrative Staff Development Program (FRAS DP) and the Department of Science and Technology – Science Education Institute (DOST-SEI) Accelerated Science and Technology Human Resource Development Program (ASTHRDP).

6. References

Akiba, T., Fukuda, K., & Suzuki, S. (2017). ChainerMN: Scalable distributed deep learning framework. Proceedings of the 31st Conference on Neural Information Processing Systems (NIPS 2017), Long Beach, California, United States, 1-7.

Carleo, G., Cirac, I., Cranmer, K., Daudet, L., Schuld, M., Tishby, N., Vogt-Maranto, L., & Zdeborova L. (2019). Machine learning and the physical sciences. Review of Modern Physics, 91, 045002. https://doi.org/10.1103/RevModPhys.91.045002

Eden, R.J., Landshoff, P.V., Olve, D.I., & Polkinghorne, J.C. (1966). The analytic S-matrix. London: Cambridge University Press

Guo, F.-K., Hanhart, C., Meißner, Ulf-G., Wang, Q., Zhao, Q., & Zou, B.-S. (2018). Hadronic molecules. Reviews of Modern Physics, 90, 015004. http://doi.org/10.1103/RevModPhys.90.015004

Guo F.-K., Hanhart C., Wang Q., & Zhao Q. (2015). Could the near-threshold XYZ states be simply kinematic effects? Physical Review D, 91, 051504(R). https://doi.org/10.1103/PhysRevD.91.051504

Kingma, D., & Ba, J. (2015) Adam: A method for stochastic optimization. Proceedings of the 3rd Conference for Learning Representations, San Diego, California, United States, 1-15.

Morgan, D. (1993) Pole counting and resonance classification. Nuclear Physics A, 543, 13. https://doi.org/10.1016/0375-9474(92)90550-4

Morgan, D., & Pennington, M.R. (1993) New data on the KK^{-} threshold region and the nature of the $f_0(S^*)$. Physical Review D, 48, 1185.

Newton, R.G. (1982). Scattering theory of waves and particles (2nd ed.). New York, United States: Springer-Verlag.

Nijmegen Group. (2005). Online repository of nucleon-nucleon scattering data. Retrieved from https://nn-online.org/NN/?page=nnphs2

Olsen, S.L., Skwarnicki, T., & Zieminska, D. (2018). Nonstandard heavy mesons and baryons: Experimental evidence. Reviews of Modern Physics, 90, 015003. https://doi.org/10.1103/RevModPhys.90.015003

Pearce, B.C., & Gibson, B.F. (1989). Observable effects of poles and shadow poles in coupled-channel systems. Physical Review C, 40, 902.

Reddi, S.J., Kale, S., & Kumar, S. (2018). On the convergence of Adam and beyond. Proceedings of the 6th International Conference on Learning Representation, Vancouver, BC, Canada, 1-23.

Rijken, T.A., & Stoks, V.G. (1996). Soft two-meson-exchange nucleon-nucleon potentials. II. One-pair and two-pair diagrams. Physical Review C, 54, 2869.

Sombillo, D.L.B. (2020). Online repository of codes used in the study. Retrieved from https://github.com/sombillo/DNN-for-bound-virtual-classification

Sombillo, D.L.B., Yoichi, I., Sato, T., & Hosaka, A. (2020). Classifying the pole of an amplitude using a deep neural network. Physical Review D, 102, 016024. https://doi.org/10.1103/PhysRevD.102.016024

Sombillo, D.L.B., Yoichi, I., Sato, T., & Hosaka A. (2021). Model independent analysis of coupled-channel scattering: A deep learning approach. Physical Review D, 104, 036001. https://doi.org/10.1103/PhysRevD.104.036001

Stoks, V.G., Klomp, R.A.M., Rentmeester, M.C.M., & de Swart, J.J. (1993). Partial-wave analysis of all nucleon-nucleon scattering data below 350 MeV. Physical Review C, 48, 792. https://doi.org/10.1103/PhysRevC.48.792

Stoks, V.G., Klomp, R.A.M., Terheggen, C.P.F., & de Swart J.J. (1994). Construction of high-quality NN potential models. Physical Review C, 49, 2950.

Taylor, J.R. (1972). Scattering theory: Quantum theory on nonrelativistic collisions. New York, United States: Dover Publications, Inc.

Tokui, S., Okuta, R., Akiba, T., Niitani, Y., Ogawa, T., Saito, S., Suzuki, S., Uenishi, K., Vogel, B., & Yamazaki, V.H. (2019). Chainer: A deep learning framework for accelerating the research cycle. Proceedings of the 25th ACM SIGKDD International Conference on Knowledge Discovery & Data Mining, Alaska, United States, 2002-2011.

Tokui, S., Oono, K., Hido, S., & Clayton, J. (2015). Chainer: A next-generation open source framework for deep learning. Proceedings of Workshop on Machine Learning Systems in the 29th Annual Conference on Neural Information Processing Systems (NIPS), Montreal, Canada, 1-6.

van Kampen, N.G. (1953). S-matrix and causality condition. II. Nonrelativistic particles. Physical Review, 91, 1267. https://doi.org/10.1103/PhysRev.91.1267

Yamaguchi, Y. (1954). Two-nucleon problem when the potential is nonlocal but separable. I. Physical Review, 95, 1628. https://doi.org/10.1103/PhysRev.95.1628

Yamaguchi, Y., Hosaka, A., Takeuchi, S., & Takizawa, M. (2020). Heavy hadronic molecules with pion exchange and quark core couplings: A guide for practitioners. Journal of Physics G: Nuclear and Particle Physics, 47, 053001. https://doi.org/10.1088/1361-6471/ab72b0